Pergamon

Int. J. Solids Structures Vol. 33, No. 3, pp. 331–342, 1996

0020-7683/96 $9.50 + .00

0020-7683(95)00047-X

FORMULATION AND IMPLEMENTATION OF THE EIGENSTRAIN METHOD EMPLOYING HIGHER ORDER ELEMENTS

D. N. DAI, D. A. HILLS and D. NOWELL
Department of Engineering Science, University of Oxford, Parks Road, Oxford OX1 3PJ, U.K.

(*Received* 13 *September* 1994)

Abstract—The analysis of three-dimensional crack problems using the eigenstrain method yields a set of hyper-singular integral equations. A key step in the numerical solution of these equations lies in the accurate evaluation of the hyper-singular terms which exist only in the finite part sense. Based on recent studies by the authors (Dai *et al.*, 1993, *J. Mech. Phys. Solids* **41**, 1003) which employ an analytical treatment of those integrals, a numerical method employing higher order non-conforming elements within the eigenstrain technique is presented here. The object is to enhance computational accuracy and efficiency. The numerical procedure is discussed in some detail, with the emphasis on evaluation of the associated singular integrals. The performance of the method is assessed by re-evaluating some well-known crack problems and comparing the results with theory where appropriate, as well as presenting some new data.

1. INTRODUCTION

The eigenstrain method has recently been established as one of the most powerful tools for accurate analysis of planar cracks of arbitrary shape in a three-dimensional elastic body. The essential idea underlying the technique is that the presence of cracks in the elastic body can be modelled by a set of eigenstrains, originating from studies of *inclusions* and *inhomogeneities* pioneered by Eshelby (1957) and developed by Mura (1982), so that the crack problem can be formulated by a set of two-dimensional hyper-singular integral equations defined over the crack face [see, for example, Murakami and Nemat-Nasser (1982), or Lee *et al.* (1987)].

In general, however, we have to resort to numerical methods to solve the hyper-singular integral equations. Needless to say, the main difficulty in the numerical solution of the hyper-singular integral equations is the accurate evaluation of the associated two-dimensional hyper-singular terms which exist only in the so-called finite part sense (Hadamard, 1952). Direct numerical calculation of the finite part integrals using a Gaussian quadrature formula has been discussed by Kutt (1975) and Ioakimidis and Pitta (1988). On the other hand, the two-dimensional hyper-singular integrals can also be interpreted in a different way, following the application of Green's theorem for plane geometries (Lin and Keer, 1987; Willis, 1992) or Stokes theorem for curved geometries (Krishnasamy *et al.*, 1990), so that the hyper-singular terms can be converted into the sum of regular contour integrals and a two-dimensional weakly singular integral. A similar strategy, very popular in the eigenstrain technique, is to evaluate the hyper-singular integral by a combination of a closed form integral (in the finite part sense) and numerical integration (Cauchy's principal value), as proposed by Murakami and Nemat-Nasser (1983). A corresponding numerical procedure employing piecewise constant elements, although incorporating a global weight function in order to model the behaviour of the displacement field near the crack front, has been developed by Murakami and Nemat-Nasser (1983), and has been successfully used by Murakami (1985), Lee and Keer (1986), Lin and Keer (1987) and Li and Hills (1990) among others, to study various crack problems. However, in our opinion, the use of higher-order elements is very desirable in order to achieve more accurate numerical solutions for an arbitrary crack geometry.

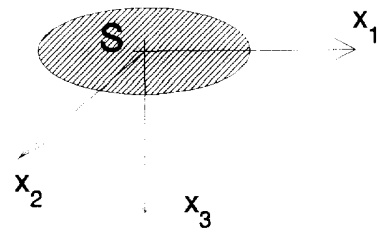

Fig. 1. Geometry of the general class of problem to be solved.

More recently, the present authors have used an analytical integration method to derive closed-form expressions for the evaluation of hyper-singular integrals (Dai *et al.*, 1993). The expressions are independent of the shape of the integration domain and the position of the singular point (except when inside the domain), thus allowing the use of higher-order non-conforming elements. The present paper addresses the formulation and implementation of the eigenstrain method employing higher-order elements, bearing in mind the arguments mentioned above. The numerical procedure is discussed in some detail for piecewise linear elements, with the emphasis on the evaluation of the associated singular integrals. The behaviour of the displacement field near the crack front is explicitly built into the interpolation function for elements adjacent to crack front, and so the stress intensity factor can be easily extracted from the displacement discontinuity solutions. The performance of the method is assessed by re-solving some well-known crack problems and comparing the results with theory where appropriate.

2. BASIC FORMULATION

In order to formulate the problem, a local Cartesian coordinate system $ox_1x_2x_3$ is fixed on the crack plane with the x_3 axis perpendicular to the crack surface, as shown in Fig. 1. The crack is modelled by dint of distributing displacement discontinuities over the crack faces, the equivalents of eigenstrain in the present case, and the resulting integral equations can be expressed as (Dai *et al.*, 1993) :

$$\int_S K_{ij}(\mathbf{x}, \mathbf{y}) b_j(\mathbf{y})\, \mathrm{d}S = -t_i^0(\mathbf{x}), \tag{1}$$

where b_j is the displacement discontinuity across the crack face in direction j, K_{ij} is the known kernel function for a given elastic infinite or semi-infinite body, and t_i^0 is the traction on the crack faces produced by the external loads applied to the elastic body but in the absence of the crack.

For an isotropic elastic half-space the kernel function K_{ij} reads as

$$\begin{aligned} K_{ij}(\mathbf{x}, \mathbf{y}) &= K_{ij}^{\infty}(\mathbf{x}, \mathbf{y}) + K_{ij}^{c}(\mathbf{x}, \mathbf{y}) \\ &= \frac{\mu}{4\pi(1-\nu)r^3}\left[(1-2\nu)\delta_{ij} + 2\nu\delta_{3i}\delta_{3j} + 3\nu\frac{r_i r_j}{r^2}\right] + K_{ij}^{c}(\mathbf{x}, \mathbf{y}), \end{aligned} \tag{2}$$

where the first term K_{ij}^{∞} is a singular function corresponding to an infinite body and K_{ij}^{c} is its image for a half-space, i.e. the corrective term to account for the presence of the free surface. The derivation of K_{ij}^{c} has been given by Dai *et al.* (1993).

Equation (1) is a set of hyper-singular boundary integral equations, and as mentioned earlier the key step in solving these equations is the accurate evaluation of the singular integrals associated with $1/r^3$, which exist only in the so-called Hadamard's finite part sense. Analytical expressions for these integrals with hyper-singular kernels have been derived recently by Dai *et al.* (1993), and for completeness the main results are summarized as follows.

As the function K_{ij}^{c} is regular we consider only the hyper-singular terms associated with K_{ij}^{s}. By adding and substracting back terms, we have

$$\int_S K_{ij}^{s}(\mathbf{x},\mathbf{y})b_j(\mathbf{y})\,\mathrm{d}S = \int_S K_{ij}^{s}(\mathbf{x},\mathbf{y})[b_j(\mathbf{y})-b_j(\mathbf{x})-b_{j,\gamma}(\mathbf{x})(y_\gamma-x_\gamma)]\,\mathrm{d}S$$
$$+b_j(\mathbf{x})\int_S K_{ij}^{s}(\mathbf{x},\mathbf{y})\,\mathrm{d}S+b_{j,\gamma}(\mathbf{x})\int_S K_{ij}^{s}(\mathbf{x},\mathbf{y})(y_\gamma-x_\gamma)\,\mathrm{d}S. \tag{3}$$

It is clear that if the density function $b_j \in C^{1,\alpha}$ $(0<\alpha\leqslant 1)$, at singular point $\mathbf{x}$, the first integral on the right-hand side of eqn (3) is at most weakly singular, where the singularity is removable so that it can be evaluated by Gaussian quadrature formula. The second integral has, of course, the same hyper-singular character as the original integral but with unit density, whereas the third integral has a singularity of order $1/r^2$ and thus exists in the Cauchy's principal value sense. As shown by Dai *et al.* (1993), the last two singular integrals can be converted into regular contour integrals. In fact, we have

$$\int_S K_{ij}^{s}(\mathbf{x},\mathbf{y})\,\mathrm{d}S = \frac{\mu}{4\pi(1-\nu)}\{[(1-2\nu)\delta_{ij}+2\nu\delta_{3i}\delta_{3j}]L+3\nu\delta_{i\alpha}\delta_{j\beta}L_{\alpha\beta}\} \tag{4}$$

and

$$\int_S K_{ij}^{s}(\mathbf{x},\mathbf{y})(y_\gamma-x_\gamma)\,\mathrm{d}S = \frac{\mu}{4\pi(1-\nu)}\{[(1-2\nu)\delta_{ij}+2\nu\delta_{3i}\delta_{3j}]M_\gamma+3\nu\delta_{i\alpha}\delta_{j\beta}M_{\alpha\beta\gamma}\}. \tag{5}$$

Here L, $L_{\alpha\beta}$, M_γ and $M_{\alpha\beta\gamma}$ are regular integrals defined over the boundary of the integration domain S:

$$L = -\int_0^{2\pi}\frac{1}{r(\theta)}\,\mathrm{d}\theta \tag{6}$$

$$L_{\alpha\beta} = -\int_0^{2\pi}\frac{\psi_\alpha\psi_\beta}{r(\theta)}\,\mathrm{d}\theta \tag{7}$$

$$M_\gamma = \int_0^{2\pi}\psi_\gamma \ln r\,\mathrm{d}\theta \tag{8}$$

$$M_{\alpha\beta\gamma} = \int_0^{2\pi}\psi_\alpha\psi_\beta\psi_\gamma \ln r\,\mathrm{d}\theta \tag{9}$$

with $\psi_\alpha = (y_\alpha-x_\alpha)/r$, and r the distance from singular point (x_1, x_2) to the boundary of S.

It is pointed out that expressions (4) and (5) hold true for any subdomain of S as long as the singular point is located *within* the subdomain rather than on its boundary. These formulae will be employed at the element level in a numerical solution and the fact that they are independent of the shape of the domain facilitates the use of higher-order non-conforming triangular or quadrilateral elements.

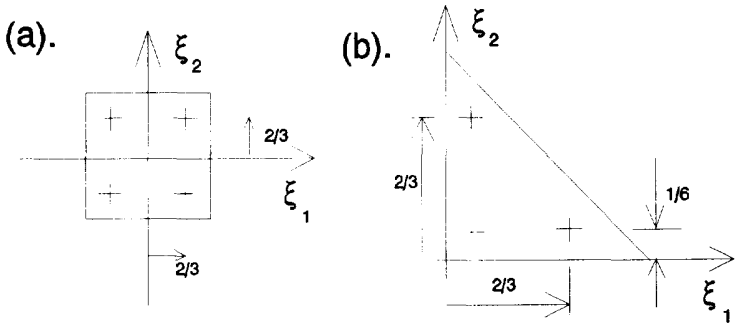

Fig. 2. Details of the non-conforming element employed.

3. NUMERICAL PROCEDURE

In setting up a numerical solution procedure for hyper-singular integral equation (1), it must be ensured that : (a) the derivatives of the density function b_j are continuous at collocation points [this smoothness requirement has been addressed by Martin and Rizzo (1989)] ; and (b) the collocation points are located *within* the element rather than on the sides of the element so that analytical expressions (4) and (5) can be employed at element level. A non-conforming element is obviously an appropriate choice to meet the above requirements, and hence we will explore it in the following discussion. Further, only a linear element is discussed here as this enables us to use the closed-form of expressions (4) and (5) (see Appendix), which dominate the evaluation of hyper-singular integral (3), and thus play a key role in producing an accurate numerical solution of hyper-singular integral equation (1). Nevertheless, the extension of the formulation to quadratic elements would be straightforward, though a numerical quadrature would have to be used to evaluate contour integrals (6)–(9).

3.1. *Discretization of domain*

The displacement discontinuity b_i is approximated in a familiar form

$$b_i = N_q(\xi) b_i^q \quad (q = 1, 2, \ldots, n_c) \tag{10}$$

within each element, where n_c is the number of collocation points which are located inside the element as shown in Fig. 2, b_i^q is the value of the displacement discontinuity at these collocation points ξ^q and N_q is the corresponding shape function, i.e.

$$N_1 = \tfrac{1}{3}(5 - 6\xi_1 - 6\xi_2) \tag{11}$$

$$N_2 = \tfrac{1}{3}(6\xi_1 - 1) \tag{12}$$

$$N_3 = \tfrac{1}{3}(6\xi_2 - 1) \tag{13}$$

for triangular elements, and

$$N_q(\xi) = \tfrac{1}{4}(1 + \tfrac{3}{2}\xi_1^q \xi_1)(1 + \tfrac{3}{2}\xi_2^q \xi_2) \quad (q = 1, 2, 3, 4) \tag{14}$$

for quadrilateral elements. In order to model the correct behaviour of the displacement field near the crack front, shape function N_q is modified by multiplying it by a given function W of the form

$$W(\xi) = \sqrt{[2d(\xi)]} \tag{15}$$

for elements adjacent to the crack front only, where d is the minimum distance from an

arbitrary point inside the element to the crack front. As function W here is defined for crack front elements only, the $C^{1,\alpha}$ continuity of the displacement discontinuity b_i within the element can be ensured.

Using approximation (10), integral equation (1) can be replaced by

$$\sum_{n=1}^{n_e} \int_{S_n} K_{ij}(\mathbf{x}, \mathbf{y}(\xi)) N_q(\xi) |J(\xi)| \, d\xi_1 \, d\xi_2 b_j^{t(n,q)} = -t_i^0(\mathbf{x}), \tag{16}$$

where n_e is the total number of elements, $t = t(n, q)$ is the global node number of the qth collocation point within the nth element and $|J| = |\partial x_\alpha / \partial \xi_\beta|$ is the determinant of the Jacobi transformation matrix.

Enforcing eqn (16) at all collocation points, we have

$$K_{ij}^{st} b_j^t = -t_i^0(\mathbf{x}^s) \quad (s, t = 1, 2, \ldots, n_d), \tag{17}$$

where n_d is the total number of collocation points, $s = s(m, p)$ is the global node number of the pth collocation point within the mth element, $\mathbf{x}^s$ is the global coordinate of collocation point s and K_{ij}^{st} is given by

$$K_{ij}^{st} = \int_{S_n} K_{ij}(\mathbf{x}^s, \mathbf{y}(\xi)) N_q(\xi) |J(\xi)| \, d\xi_1 \, d\xi_2. \tag{18}$$

Equation (18) represents a system of algebraic equations which can be solved by standard Gaussian elimination methods.

3.2. *Calculation of matrix elements* $K_{ij}^{s(m,p),t(n,q)}$

To evaluate the matrix elements K_{ij}^{st}, two cases need to be taken account of separately, depending on the position of the collocation point.

Case 1 : m ≠ n. In this case the integral is regular as the collocation point $\mathbf{x}^s$ lies outside the integral domain S_n in integral (18) so that it can be calculated numerically by a standard Gaussian quadrature formula as follows (Zienkiewicz, 1977) :

$$K_{ij}^{st} = \sum_{g=1}^{n_1} \sum_{h=1}^{n_2} w_g w_h K_{ij}(\mathbf{x}^s, \mathbf{y}(\xi^{gh})) N_q(\xi^{gh}) |J(\xi^{gh})|, \tag{19}$$

where n_α is the number of Gauss points in the ξ_α direction, $\xi^{gh} = (\xi_1^g, \xi_2^h)$ is the coordinate of the $g \times h$ Gauss point, and w_g and w_h are the associated weighting factors. To enhance the computational efficiency and accuracy in a numerical implementation, the number of Gauss points is not fixed, but varies with the distance from the collocation point to the element. A modification of the criterion given by Lachat and Watson (1976) can be used for this purpose. If this criterion is not achieved, the domain of integration is subdivided and the Gaussian quadrature formula (19) is applied to each subdomain.

It is pointed out that the triangle has to be transformed into a standard square in order to apply formula (19) to triangular elements.

Case 2 : m = n. As we can see from eqn (2), the integrand K_{ij} in eqn (18) has contributions from both K_{ij}^s and K_{ij}^r. The latter is a regular function so that Gaussian quadrature formula (19) can still be used to evaluate this part of the integral; but the integral associated with K_{ij}^s is hyper-singular as the collocation point lies within the the integral area S_n. Its numerical evaluation has to be performed in terms of eqns (3)–(5) except that the density b_j is replaced by its interpolation function N_q and the domain of integration is limited to the element under consideration, i.e.

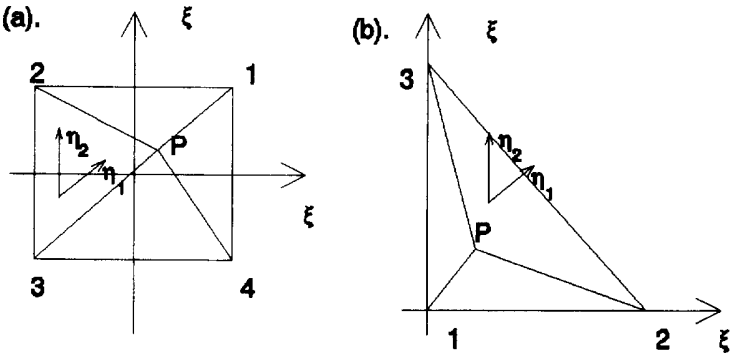

Fig. 3. Sub-division of the elements needed to evaluate the weakly singular integral.

$$K_{ij}^{sl} = \int_{S_n} K_{ij}^{s}(\mathbf{x}^{s}, \mathbf{y}(\xi))[N_q(\xi) - N_q(\xi^p) - N_{q,\gamma}(\xi^p)(y_\gamma - x_\gamma^s)]|J(\xi)|\,\mathrm{d}\xi_1\,\mathrm{d}\xi_2$$
$$+ N_q(\xi^p)\int_{S_n} K_{ij}^{s}(\mathbf{x}^{s}, \mathbf{y})\,\mathrm{d}S + N_{q,\gamma}(\xi^p)\int_{S_n} K_{ij}^{s}(\mathbf{x}^{s}, \mathbf{y})(y_\gamma - x_\gamma^s)\,\mathrm{d}S, \quad (20)$$

where ξ^p is the local coordinate of collocation point $\mathbf{x}^{s(m,p)}$, and the contribution from K_{ij}^{c} has been ignored. The second and third integrals on the right-hand side of eqn (20) can be evaluated by the results embodied in eqns (4) and (5) and in the present case closed-forms are available (see Appendix), whereas the first integral is weakly singular and can be evaluated using the following strategy. To simplify the description, this integral is rewritten as

$$I = \int_{S_n} \frac{F(\xi_1, \xi_2)}{\rho}\,\mathrm{d}\xi_1\,\mathrm{d}\xi_2, \quad (21)$$

where $\rho = |\xi - \xi^p|$ and $F(\xi_1, \xi_2)$ is the product of the original integrand and ρ. Hence it is bounded and continuous at ξ^p. The $1/\rho$ singularity of the integral is explicitly expressed here. To evaluate this integral we divided the domain of integration into four or three triangles as shown in Fig. 3, and each triangle is transformed into a square, again using a degenerate mapping. For example, for triangle $\triangle_{12p}$ in Fig. 3(a), the corresponding coordinate transformation is

$$\xi_1 = \tfrac{1}{2}\eta_1(1+\eta_2) + \tfrac{1}{2}(1-\eta_2)\xi_1^p \quad (22)$$

$$\xi_2 = \tfrac{1}{2}(1+\eta_2) + \tfrac{1}{2}(1-\eta_2)\xi_2^p \quad (23)$$

so that the contribution from this triangle to the integral I is

$$I_1 = \int_{-1}^{1}\int_{-1}^{1} \frac{\bar{F}(\eta_1, \eta_2)(1-\xi_2^p)}{2[(\eta_1 - \xi_1^p)^2 + (1-\xi_2^p)^2]^{1/2}}\,\mathrm{d}\eta_1\,\mathrm{d}\eta_2, \quad (24)$$

where the singularity of the integrand has been removed. Hence the standard Gaussian quadrature formula (19) can be employed again for its numerical evaluation. Integrations over the remaining triangles can be treated in the same way. This strategy to remove the singularity is a simple extension of the method proposed by Lachat and Watson (1976), where the collocation point is located on the corner or midside of the element.

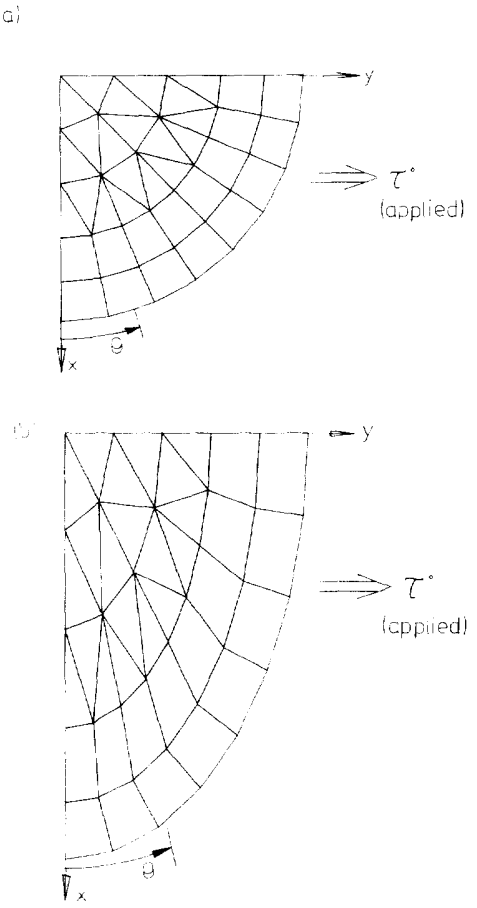

Fig. 4. Meshes used in the analysis of elliptical cracks : (a) $a/b = 1$; (b) $a/b = 1.5$.

4. NUMERICAL RESULTS

The method described in the preceding section has been employed to re-solve several well-known crack problems so that its performance might be assessed. Further, growth analysis of a surface-breaking crack has been carried out to demonstrate the versatility of the method, where it is assumed that the crack tends to evolve into a shape which produces a constant stress intensity factor around the front.

4.1. *An elliptical crack in an infinite body*

Consider an elliptical crack in an infinite body which suffers a remote uniform tension σ^0 perpendicular to the crack plane and a uniform shear traction τ^0 parallel to the minor axis of the ellipse. This is, of course, a well-known problem possessing an exact answer. Also, it has been treated by the eigenstrain method before, but employing a global weight function which incorporates the known asymptotic behaviour around the crack front. In this formulation, we will not employ this strategy, but use the standard weighting function, applied to the crack front elements only [eqn (15)], as if the crack had an arbitrary shape. This therefore represents a fairer test of the scheme, when it is to be used to study cracks of more complex shape. Because of the symmetry of the problem only one-quarter of the domain needs to be discretized, and typical meshes employed are shown in Fig. 4 with 36 elements and 124 collocation points. The variations of dimensionless stress intensity factors $K_I/\sigma^0\sqrt{(\pi b)}$, $K_{II}/\tau^0\sqrt{(\pi b)}$ and $K_{III}\ \tau^0\sqrt{(\pi b)}$ along the crack front are plotted in Fig. 5 for $a/b = 1, 1.5, 2$, together with the corresponding analytical solution (Kassir and Sih, 1966), where Poisson's ratio is set to 0.3. It is observed that the numerical procedure gives very accurate solutions. The maximum error, which occurs in K_{III} when $a/b = 2$, is less than 1.8%.

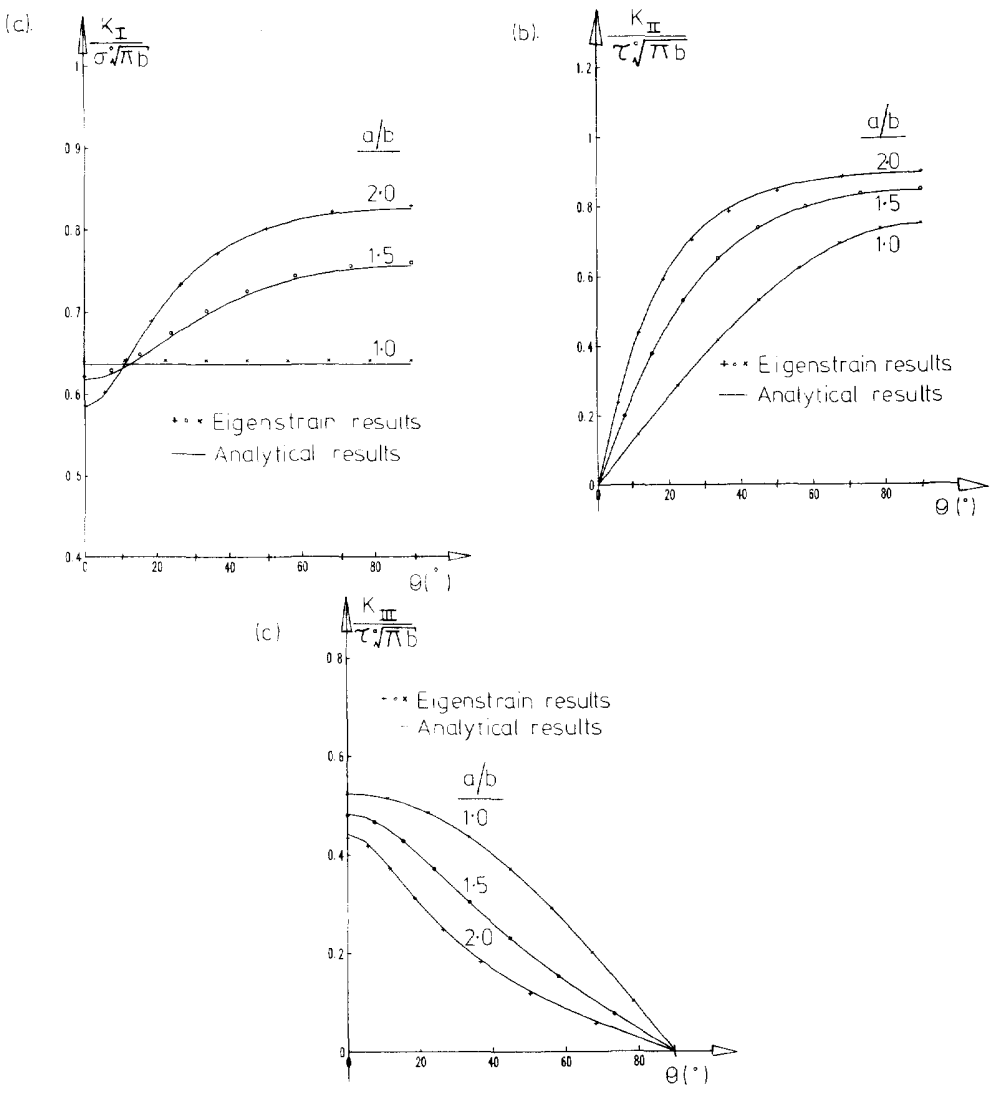

Fig. 5. Variation of stress intensity factors occurring around the crack front for the geometry of Fig. 4.

4.2. *A square crack in an infinite body*

A square crack in an infinite body suffering a remote uniform tension σ^0 perpendicular to the crack faces and a uniform shear traction τ^0 parallel to one pair of sides is considered. It provides another vehicle for testing the procedure, which provides valuable insight into its power and characteristics.

A quarter of the square is idealized by a 6×6 mesh with 35 elements, see Fig. 6, where the side AB represents the direction in which the shear traction is applied. The opening mode stress intensity factor at point A, where the maximum occurs, is listed in Table 1 (this was actually found from a 10×10 mesh), together with other results available in the literature (Mastrojannis *et al.*, 1979 ; Murakami and Nemat-Nasser, 1983 ; Isida *et al.*, 1993). It is seen that all results are in close agreement.

This example provides an excellent opportunity to study the convergence of the proposed numerical procedure as the mesh can be uniformly and systematically refined. To this end, meshes at various levels of refinement are employed and a comparison of the corresponding results is made in Table 2 which clearly demonstrates the convergence characteristics. It is not surprising that a moderate mesh can produce very accurate results, as the displacement field near the crack front was correctly modelled and hyper-singular integrals were evaluated largely in closed-form.

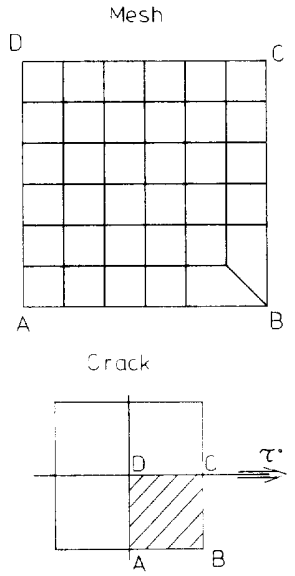

Fig. 6. Geometry of the problem : a square crack in an infinite body subject to uniform far-field tension and shear traction.

Table 1. Comparison of stress intensity factors at point A or C of a square crack

Authors	$K_I/\sigma^0\sqrt{(\pi a)}$
Present authors	0.7550
Mastrojannis *et al.* (1979)	0.745
Murakami and Nemat-Nasser (1983)	0.736
Isida *et al.* (1993)	0.7533

4.3. *Growth analysis of a surface-breaking crack*

Consider a surface-breaking crack in a half-space which is subject to a remote, uniform, cyclic tension σ^0, such that the crack grows by fatigue. There is considerable evidence, both experimental and theoretical, to support the thesis that such flaws grow and develop so as to give rise to a constant stress intensity factor around the front [see, for example, Gilchrist *et al.* (1992)]. It is interesting to speculate on the development of the shape of cracks as they progress towards this condition. This is also of practical interest as it means that, under some conditions, the subsurface shape of a crack may be inferred from the surface-breaking length alone.

In this example, we take the initial shape of the crack to be a semi-circle (thumbnail), and to avoid the difficulty of the change of order of singularity close to the free surface the

Table 2. Convergence studies of stress intensity factors for a square crack

Mesh	$K_I/\sigma^0\sqrt{(\pi a)}$(A)	$K_{II}/\tau^0\sqrt{(\pi a)}$(C)	$K_{III}/\tau^0\sqrt{(\pi a)}$(A)
6 × 6	0.75557	0.84680	0.65986
7 × 7	0.75532	0.84659	0.65967
8 × 8	0.75517	0.84645	0.65955
9 × 9	0.75505	0.84635	0.65947
10 × 10	0.75498	0.84629	0.65941

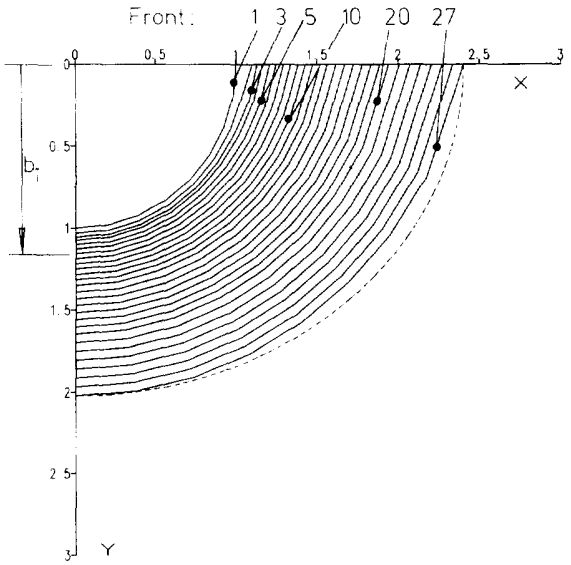

Fig. 7. Evolution of the crack front shape for a semi-circular surface-breaking crack subject to uniform far-field tension.

Poisson's ratio is set to zero.† The stress intensity is calculated at all nodal points on the present crack front, and then a crack growth condition similar to the Paris law, i.e.

$$\delta a = C\left(\frac{K_I - K_{IC}}{K_{IC}}\right)^m,$$

where C and m are material constants and K_{IC} is the fracture toughness of the material, is employed to predict the new position of these nodes, thus generating a new crack front. The positions of the crack front at various instants as the crack depth grows from b to around $2b$ are depicted in Fig. 7. Also shown, by the dotted line on the figure, is an ellipse, fitted through the same end points. It may be seen that the final shape is not quite semi-elliptical in form. The variations of dimensionless stress intensity factor along the crack front at selected instants, corresponding to some of the crack fronts shown in Fig. 7, are plotted in Fig. 8. This clearly shows that evolution towards a constant-K solution is well-advanced after three progressions of the crack front, and thereafter progressive refinement towards such a state occurs rather gradually; this is also apparent from Fig. 7, where it may be seen that the lines denoting the crack front become almost parallel quite quickly. Also shown in Fig. 8 is the variation in crack tip stress intensity factor around the crack front for a semi-elliptical crack. Note that the graph has a false origin.

5. CONCLUSION

Based on our recent work on the eigenstrain method, especially on an analytical treatment for the associated hyper-singular integral, we have developed a numerical procedure using linear non-conforming elements within the eigenstrain technique. As the correct behaviour of the displacement field near the crack front has been explicitly incorporated in the associated elements, the stress intensity factors can be abstracted accurately and directly. A numerical scheme for the evaluation of the weakly singular integral which arises has been detailed, and a closed form solution for those contour integrals needed has also been given (Appendix). Numerical tests have shown that accurate solutions can be

†It is known that the order of singularity obtaining where a crack front breaks a free surface is dependent on the value of Poisson's ratio and on the angle between the crack front and the surface. In general the singularity is weaker than $r^{-1/2}$. However, if ν is chosen to be zero this problem is obviated, as the strength of the singularity remains unchanged.

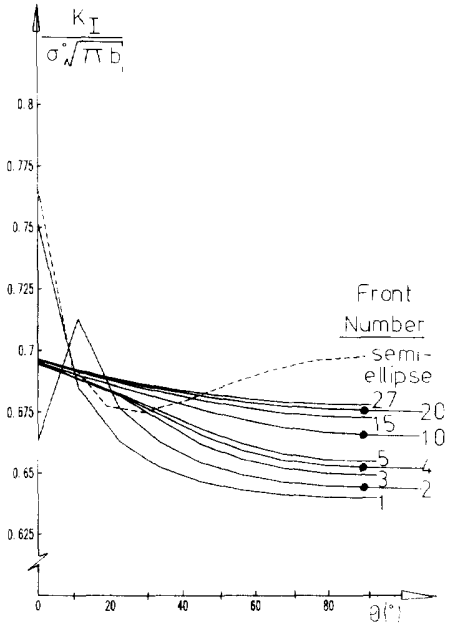

Fig. 8. Variation of stress intensity factor around the crack front for various positions of the front, and a comparison with the solution obtained when the crack is semi-elliptical in shape.

achieved by the method proposed and convergence of the solutions can also be anticipated even when only a moderately refined mesh is used.

Acknowledgement—D. N. Dai would like to acknowledge the support of the SERC under contract No. GR/J53942.

REFERENCES

Dai, D. N., Nowell, D. and Hills, D. A. (1993). Eigenstrain methods in three-dimensional crack problems : an alternative integration procedure. *J. Mech. Phys. Solids* **41,** 1003–1017.

Eshelby, J. D. (1957). The determination of the elastic field of an ellipsoidal inclusion and related problems. *Proc. R. Soc.* **A241,** 376–396.

Gilchrist, M. D., Chipalo, M. I. and Smith, R. A. (1992). Shape development of surface defects in tension fatigued finite thickness plates. *Int. J. Vessels Piping* **49,** 121–137.

Hadamard, J. (1952). *Lectures on Cauchy's Problem in Linear Partial Differential Equations*. Dover Publications, New York.

Ioakimidis, N. I. and Pitta, M. S. (1988). Remarks on the gaussian quadrature rule for finite-part integrals with a second-order singularity. *Comp. Methods Appl. Mech. Engng* **69,** 325–343.

Isida, M., Tsuru, H. and Noguchi, H. (1993). An analysis for three dimensional cracks. *Fatigue Fracture Engng Structures* **17,** 739–748.

Kassir, M. K. and Sih, G. C. (1966). Three-dimensional stress distribution around an elliptical crack under arbitrary loadings. *J. Appl. Mech., ASME* **33,** 601–611.

Krishnasamy, G., Schmerr, L. W., Rudolphi, T. J. and Rizzo, F. J. (1990). Hypersingular boundary integral equations : some applications in acoustic and elastic wave scattering. *J. Appl. Mech., ASME* **57,** 404–414.

Kutt, H. R. (1975). The numerical evaluation of principal value integrals by finite-part integration. *Numer. Math.* **24,** 200–210.

Lachat, J. G. and Watson, J. O. (1976). Effective numerical treatment of boundary integral equations : a formulation for three-dimension elastostatics. *Int. J. Numer. Meth. Engng* **10,** 991–1005.

Lee, J. C., Farris, T. N. and Keer, L. M. (1987). Stress intensity factors for cracks of arbitrary shape shape near an interfacial boundary. *Engng Fracture Mech.* **27,** 27–41.

Lee, J. C. and Keer, L. M. (1986). Study of a three-dimensional crack terminating at an interface. *ASME, J. Appl. Mech.* **53,** 311–316.

Li, Yingzhi and Hills, D. A. (1990). The analysis of three-dimensional cracks generated by sharp indentation. *J. Mech. Phys. Solids* **38,** 255–272.

Lin, W. and Keer, L. M. (1987). Scattering by a planar three-dimensional crack. *J. Acoust. Soc. Am.* **82,** 1442–1448.

Martin, P. A. and Rizzo, F. J. (1989). On boundary integral equations for crack problems. *Proc. R. Soc.* **A421,** 341–355.

Mastrojannis, E. N., Keer, L. M. and Mura, T. (1979). Stress intensity factor for a plane crack under normal pressure. *Int. J. Fracture* **15,** 247–258.

Mura, T. (1982). *Micromechanics of Defects in Solids*. Martinus Nijhoff, Dordrecht.

Murakami, Y. (1985). Analysis of stress intensity factors of mode I, II and III for inclined surface cracks of arbitrary shape. *Engng Fracture Mech.* **22,** 101–114.
Murakami, Y. and Nemat-Nasser, S. (1982). Interacting dissimilar semi-elliptical surface flaws under tension and bending. *Engng Fracture Mech.* **16,** 373–386.
Murakami, Y. and Nemat-Nasser, S. (1983). Growth and stability of interacting surface flaws of arbitrary shape. *Engng Fracture Mech.* **17,** 193–210.
Willis, J. R. (1992). Private communication.
Zienkiewicz, O. C. (1977). *The Finite Element Method*, 3rd edn. McGraw-Hill, New York.

APPENDIX: CLOSED FORM OF CONTOUR INTEGRALS L, $L_{\alpha\beta}$, M_γ AND $M_{\alpha\beta\gamma}$

For a linear triangular and quadrilateral element, contour integrals L, $L_{\alpha\beta}$, M_γ and $M_{\alpha\beta\gamma}$ can be expressed in closed form. The expressions for L and $L_{\alpha\beta}$ have been given by Dai *et al.* (1993) and for completeness they are reproduced here together with the expressions of M_γ and $M_{\alpha\beta\gamma}$. Due to the symmetrical property $L_{\alpha\beta} = L_{\beta\alpha}$, $M_{\alpha\beta\gamma} = M_{\beta\alpha\gamma} = M_{\alpha\gamma\beta}$ and the relationship $L_{\alpha\alpha} = L - L_{\beta\beta}$, $M_{\alpha\alpha\gamma} = M_\gamma - M_{\alpha\beta\beta}(\alpha \neq \beta)$, only those independent components are given here.

$$L = \sum_{i=1}^{n} \frac{1}{a_i}[\cos\theta_{i+1} - \cos\theta_i + k_i(\sin\theta_{i+1} - \sin\theta_i)] \tag{A1}$$

$$L_{11} = \sum_{i=1}^{n} \frac{1}{3a_i}[\cos^3\theta_{i+1} - \cos^3\theta_i + k_i(3\sin\theta_{i+1} - 3\sin\theta_i - \sin^3\theta_{i+1} + \sin^3\theta_i)] \tag{A2}$$

$$L_{12} = \sum_{i=1}^{n} \frac{1}{3a_i}[-\sin^3\theta_{i+1} + \sin^3\theta_i + k_i(-\cos^3\theta_{i+1} + \cos^3\theta_i)] \tag{A3}$$

$$M_1 = \sum_{i=1}^{n} -\frac{k_i}{\sqrt{(1+k_i^2)}} I \tag{A4}$$

$$M_2 = \sum_{i=1}^{n} \frac{1}{\sqrt{(1+k_i^2)}} I_i \tag{A5}$$

$$M_{121} = \sum_{i=1}^{n} \frac{1}{3(1+k_i^2)}\left[-\cos\theta_{i+1} + \cos\theta_i + k_i(\sin\theta_{i+1} - \sin\theta_i) + \frac{1}{\sqrt{(1+k_i^2)}} I_i\right] \tag{A6}$$

$$M_{122} = \sum_{i=1}^{n} \frac{k_i}{3(1+k_i^2)}\left[-\cos\theta_{i+1} + \cos\theta_i + k_i(\sin\theta_{i+1} - \sin\theta_i) - \frac{k_i^2}{\sqrt{(1+k_i^2)}} I_i\right], \tag{A7}$$

where n is the number of sides of the element and a_i, k_i, θ_i and I_i are defined as follows:

$$a_i = x_2^i - x_2^0 - k_i(x_1^i - x_1^0)$$

$$k_i = \frac{x_2^{i-1} - x_2^i}{x_1^{i-1} - x_1^i}$$

$$\theta_i = \tan^{-1}\frac{x_2^i - x_2^0}{x_1^i - x_1^0}$$

$$I_i = \ln\frac{(\cos\theta_{i+1} + k_i\sin\theta_{i+1} + \sqrt{(1+k_i^2)})r_{i+1}}{(\cos\theta_i + k_i\sin\theta_i + \sqrt{(1+k_i^2)})r_i}$$

in which r_i is the distance from collocation point (x_1^0, x_2^0) to the ith node (x_1^i, x_2^i), and $x_\alpha^{n+1} = x_\alpha^1$.